Analytical and Bioanalytical Chemistry
https://doi.org/10.1007/s00216-019-02042-3

RESEARCH PAPER

An efficient turn-on fluorescence biosensor for the detection of glutathione based on FRET between N,S dual-doped carbon dots and gold nanoparticles

Wenjuan Dong[1] · Ruiping Wang[1] · Xiaojuan Gong[1] · Chuan Dong[1]

Received: 31 May 2019 / Revised: 11 July 2019 / Accepted: 17 July 2019

Abstract

Fluorescence resonance energy transfer (FRET) is a kind of energy transfer mechanism depending on the distance between donor and acceptor, which exhibited potential application in biosensors. In this study, an efficient fluorescence "turn-on" strategy for the detection of glutathione (GSH) has been established based on FRET between nitrogen and sulfur dual-doped carbon dots (N,S-CDs) and gold nanoparticles (Au NPs). A novel N,S-CDs was synthesized by a one-pot hydrothermal treatment of 3-aminothiophenol, which possessed excellent fluorescence property with the maximum emission wavelength of 530 nm. Then, the as-prepared N,S-CDs served as energy donor to transfer energy to Au NPs via FRET process, resulting in fluorescence quenching of N,S-CDs. However, the fluorescence of N,S-CDs was recovered efficiently by adding GSH into the mixture solution of N,S-CDs and Au NPs. Therefore, the FRET assembly of N,S-CDs and Au NPs was used as a fluorescence probe for the "turn-on" sensing GSH with the linear range from 3.8 to 415.1 μM and the limit detection of 0.21 μM. This nanosensor platform was employed to monitor GSH in serum samples with satisfying results.

Keywords N,S dual-doped carbon dots · Gold nanoparticles · Fluorescence resonance energy transfer · Glutathione

Introduction

Glutathione (GSH), as imperative antioxidant and the most abundant intracellular thiol, plays an important role in physiological functions including sustaining intracellular redox liveness, cellular regulation, healthy metabolism, and intracellular signal deliver [1]. The abnormality of GSH level in the human body is associated with some diseases, such as Parkinson's disease, dementia, liver damage, cancer, Alzheimer's disease, and neurodegenerative disorders [2, 3]. Due to its biological significance, great efforts have been devoted to establishing diverse approaches for sensitive and selective determination of GSH, including electrochemistry [4], high-performance liquid chromatography [5], surface enhanced Raman scattering [6], colorimetric [7], mass spectrometry [8], capillary electrophoresis [9], enzyme-linked immunosorbent assay [10], and fluorescence spectroscopy [11, 12]. Among them, fluorescence detection has received sustaining attentions attributing to its distinguished advantages in terms of rapid response, simple operation, low-cost instrument, and abundant analysis strategies. A large number of fluorescent probes including organic dyes [13] and polymeric materials [14] have been successfully used to detect GSH, but some shortcomings such as weak fluorescence, complicated labeling, intricate synthesis process, high environmental hazard, or cytotoxicity limit their practical applications. Therefore, fluorescent nanomaterials as an excellent substitute for traditional fluorescent dyes have been employed for the detection of GSH [15, 16]. However, the similar structure of biothiols such as cysteine (Cys) and homocysteine (Hcy) cause serious interference in the selective detection of GSH [17, 18]. Thus, a

Electronic supplementary material The online version of this article (https://doi.org/10.1007/s00216-019-02042-3) contains supplementary material, which is available to authorized users.

✉ Wenjuan Dong
wjdong@sxu.edu.cn

✉ Xiaojuan Gong
gxj1124@sxu.edu.cn

[1] Institute of Environmental Science, and School of Chemistry and Chemical Engineering, Shanxi University, 92 Wu Cheng Road, Taiyuan 030006, Shanxi, China

Published online: 12 August 2019

great challenge still remains in developing a simple, low-cost, highly sensitive, with good selectivity, and excellent anti-interference fluorescence method for discriminative recognition of GSH over Cys and Hcy.

Fluorescence resonance energy transfer (FRET) is an orientation-dependent non-radiative energy transfer process [19–21]. The occurrence of FRET is very susceptible to the distance between donor and acceptor because the energy can be effectively transferred from the donor to the acceptor only when the distance between them is less than 100 Å [22]. It makes FRET become a beneficial technique for designing fluorescence sensing platforms. In order to increase the FRET efficiency and improve the sensor sensitivity, it is necessary to obtain an outstanding donor-acceptor FRET pair in sensing system. Currently, carbon dots (CDs) have aroused intense attentions due to their unique properties including low-cost, small size, fine chemical inertness, facile functionalization, outstanding photochemical stability, high water solubility, tunable excitation/emission wavelength, good biocompatibility, and low cytotoxicity [23–25]. Furthermore, compared with other carbon-based nanomaterials, CDs could be prepared by many raw materials and endowed extraordinarily good water dispersity. These extraordinary properties make CDs as an ideal energy donor in FRET-based biosensors [26]. Gold nanoparticles (Au NPs) can be used as a fluorescence quencher due to their high quenching efficiency within a wide absorbance spectral range which could precisely overlap the emission spectra of CDs [27] and then result in the occurrence of FRET. FRET based on /CDs/Au NPs system has been extensively applied for the detection of small molecule [28], ion [29], and DNA [30, 31]. However, some of the donor-acceptor pairs faced the disadvantage of poor energy transfer efficiency, and the "turn-on" fluorescence sensing platform had a low recovery. Hence, it is still necessary to establish a high-efficient FRET system and fluorescence recovery for detecting GSH in order to improve its sensitivity.

In this work, we designed a novel "turn-on" fluorescence biosensor for the determination of GSH based on FRET system of N,S-CDs and Au NPs. N,S-CDs was synthesized by a one-pot hydrothermal treatment of 3-aminothiophenol, which contained abundant amino groups on the surface of N,S-CDs and led to a positive potential. After adding Au NPs into the N,S-CD solution, the negatively charged Au NPs were closed to the N,S-CDs by electrostatic interaction, resulting in the occurrence of FRET and the fluorescence quenching of N,S-CDs. Then, with the addition of GSH into the FRET system, the fluorescence of N,S-CDs was restored and the recovery degree of fluorescence intensity was linearly related to the concentration of GSH. Based on this mechanism, a novel fluorescent nanosensor for detecting GSH with high sensitivity and selectivity was constructed, which was also successfully applied to the detection of GSH in real samples. The working principle is illustrated in Scheme 1.

Experimental

Reagents

Hydrogen tetrachloroaurate(III) trihydrate ($HAuCl_4 \cdot 3H_2O$, 99.9+%) was acquired from Aldrich (Milwaukee, WI, USA). Sodium citrate ($C_6H_5Na_3O_7 \cdot 2H_2O$), 3-aminothiophenol ($C_6H_7NS$), glutathione (GSH), L-histidine (L-His), L-cysteine (L-Cys), and other amino acids were obtained from Aladdin Chemical Co. Ltd. (Shanghai, China). Disodium hydrogen phosphate ($Na_2HPO_4 \cdot 12H_2O$), sodium dihydrogen phosphate ($NaH_2PO_4 \cdot 2H_2O$), and ethanol were obtained from Tianjin Chemical Plant (Tianjin, China). All reagents were of analytical grade or above, which were used as received without further purification.

Equipment

The morphology and size of N,S-CDs and Au NPs were obtained by transmission electron microscopy (TEM) and high-resolution transmission electron microscopy (HRTEM) images using a JEOL JEM-2100F transmission electron microscopy (Tokyo, Japan). Photoluminescence spectra were recorded on a Model FP-8300 spectrometer (JASCO, Japan) with both excitation and emission slits setting at 10 nm. UV-vis absorption spectra were recorded on a Lambda 365 UV-vis absorption spectrophotometer (PerkinElmer, USA). The Fourier transform infrared spectra (FTIR) were acquired on a Bruker Tensor II FTIR spectrometer (Bremen, Germany). All pH were made with a PB-10 pH meter (Sartorius Scientific Instrument (Beijing) Co., Ltd., China). The zeta potential was recorded on zeta potential and particle size analyzer (Malvern, Nano ZS 90).

Synthesis of N,S-CDs

N,S-CDs was synthesized by a one-pot hydrothermal treatment of 3-aminothiophenol. Typically, 0.1 g of 3-aminothiophenol was dissolved in 20 mL of ethanol. Then the solution was transferred into a 50-mL Teflon-lined stainless steel autoclave and heated at 180 °C for 12 h. After cooling down the room temperature naturally, the purplish red solution was obtained. The solution was evaporated by rotary evaporator and re-dispersed in 2.0 mL ethanol and 18.0 mL double-distilled water. The purplish red solution was dialyzed 48 h using dialysis membrane of a molecular weight cut off (MWCO) of 500–1000 Da and then centrifuged at 8000 rpm for 10 min to gather the supernatant. Ultimately, the obtained supernatant was lyophilized to obtain the dry N,S-CDs product.

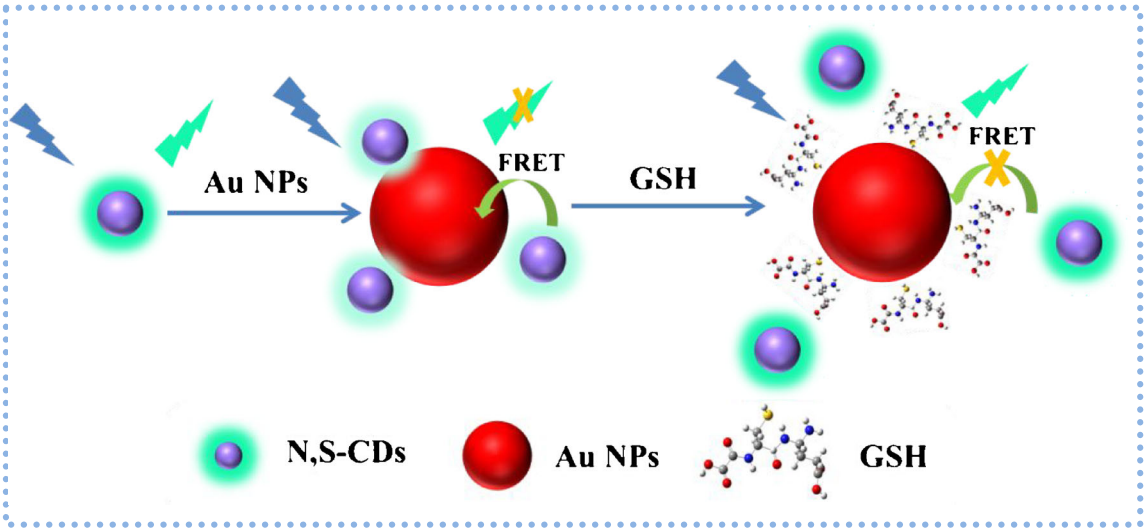

Scheme 1 Schematic principle for the determination of GSH based on FRET of N,S-CDs and Au NPs

Fabrication of Au NPs

Au NPs were prepared using citrate sodium as a reducing reagent according to previous report [32] with a slight modification. Briefly, 10 mL of 1 mM $HAuCl_4$ aqueous solution was heated to boil, and then 1 mL of 38.8 mM freshly sodium citrate solution was rapidly added under vigorous magnetic stirring. The reaction was kept for 20 min until the color of the solution was changed from yellow to wine-red. The solution was then cooled to room temperature and then stored at 4 °C for further use.

Determination of GSH

Firstly, 2.5 mL PBS buffer (pH 5.0, 10 mM) and Au NPs (150 μL, 14 nM) were respectively added to 10 μL the prepared N,S-CDs solution (5 mg mL^{-1}) and incubated for 5 min under sufficient stirring. Then, various concentrations of GSH were mixed with N,S-CDs/Au NPs solution and incubated for another 15 min. The fluorescence spectra were recorded with the excitation wavelength of 460 nm. The process for all the optimization and control experiments were handled according to the above procedure.

The detection of GSH in real samples

The human serum samples of healthy candidates were obtained from the Hospital of Shanxi University. The collected samples were centrifuged at 8000 r min^{-1} for 15 min to remove impurities and diluted into 25 times. The standard addition method was applied to assess the practicability of the nanosensor platform. Concentrations of 0, 3.77, 7.55, and 15.09 μM GSH were added into the diluted human serum sample. And the detection process was handled according to the "Determination of GSH" section.

Results and discussion

Characterization of the as-prepared N,S-CDs and Au NPs

TEM and HRTEM images were applied to characterize the size and morphology of the as-prepared N,S-CDs. As shown in Fig. 1a, the N,S-CDs were nearly spherical dots and well dispersed in the copper grid. The inset of Fig. 1a revealed that the particle size of N,S-CDs was distributed in the range of 1.2–4.4 nm with an average size of 3.0 ± 0.4 nm. The HRTEM image (Fig. 1b) displayed that the N,S-CDs possessed high crystallinity with the lattice spacing of 0.20 nm, which was similar to a graphitic structure. The FTIR spectra of N,S-CDs (see Electronic Supplementary Material (ESM) Fig. S1) displayed a characteristic absorption band of S–H stretching vibrations at 2587 cm^{-1}. And the absorption peaks at 3429, 3211, and 1587 cm^{-1} suggested that the N,S-CDs exist –OH, –NH, and C=O groups. The peaks at 3046, 2820, and 1476 cm^{-1} corresponded to the C–H bond. The UV and fluorescence spectra were investigated and presented in Fig. 2. It can be seen from the UV-vis absorption spectra of N,S-CDs (red line in Fig. 2a) that N,S-CDs possessed two absorption peaks at 298 and 354 nm which was consistent with the $n \rightarrow \pi^*$ transition of the C=O bond and the excited defect surface states caused by the N and S heteroatoms, respectively. The blank line in Fig. 2a was the excitation spectrum of N,S-CDs, which can be observed that the excitation peaks were located at 335, 370, and 460 nm, respectively. The blue, green, and pink lines in Fig. 2a were the emission spectra of N,S-CDs with the excitation wavelength of 335, 370, and 460 nm, respectively. The maximum fluorescence emission intensity can be obtained when it was excited at 460 nm. The optical images of N,S-CDs under daylight and UV irradiation were shown in the inset of Fig. 2a, indicating it emitted strong green

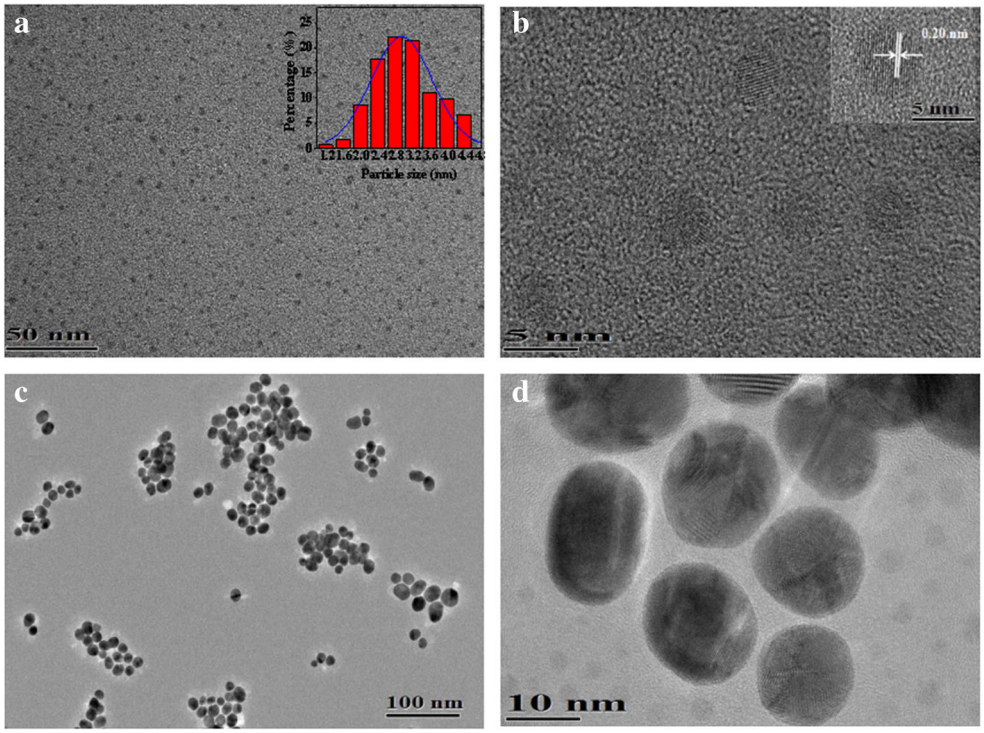

Fig. 1 TEM and HRTEM images and particle size distribution histogram of the as-prepared N,S-CDs (**a**, **b**) and Au NPs (**c**, **d**)

fluorescence under 365 nm UV light. Fig. 2b displayed the fluorescent behavior of N,S-CDs under different excitation wavelengths from 340 to 500 nm. It can be seen that the maximum emission peaks remained constant at ca. 530 nm, demonstrating the N,S-CDs possessed excitation-independent fluorescent behavior which may be attributed to the $\pi^* \rightarrow \pi$ transitions of the graphitic structure [33].

The typical TEM and HRTEM images of the as-prepared Au NPs were shown in Fig. 1c, d, respectively. Fig.1c demonstrated that the Au NPs were spherical, monodisperse, and fairly uniform with an average size of about 13.0 ± 1.5 nm. The UV-visible spectrum of Au NPs (black line in Fig. 3a) depicted the typical surface plasmon resonance absorbance peak at 520 nm. The concentration of Au NP solution was estimated to be 14 nM according to Beer's law.

FRET system construction between N,S-CDs and Au NPs

It is generally known that the efficiency FRET must meet two significant factors. One factor is that the emission spectra of the donor should overlap to some extent with the absorption spectra of the acceptor. The other factor is that the distance between the donor and the acceptor should be comparable to the dimensions of most biology macromolecules about10 to 100 Å [22]. The fluorescence of N,S-CDs and the absorption

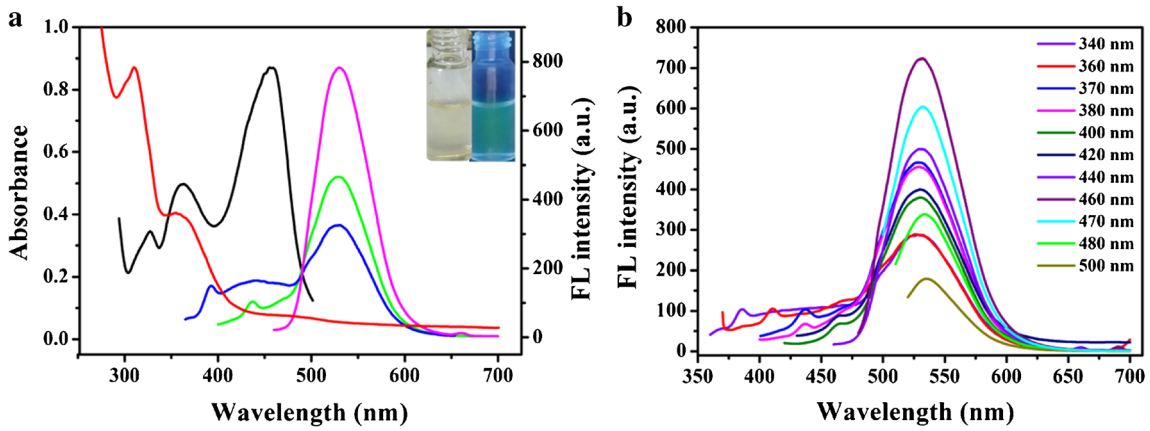

Fig. 2 **a)** The UV-visible absorbance (red line) and excitation (blank line) and emission (blue, green, and pink lines) spectra of N,S-CDs. The inset is the photographs of N,S-CDs under natural light and 365 nm UV light. **b)** The fluorescence emission spectra of N,S-CDs at different excitation wavelengths from 340 to 500 nm

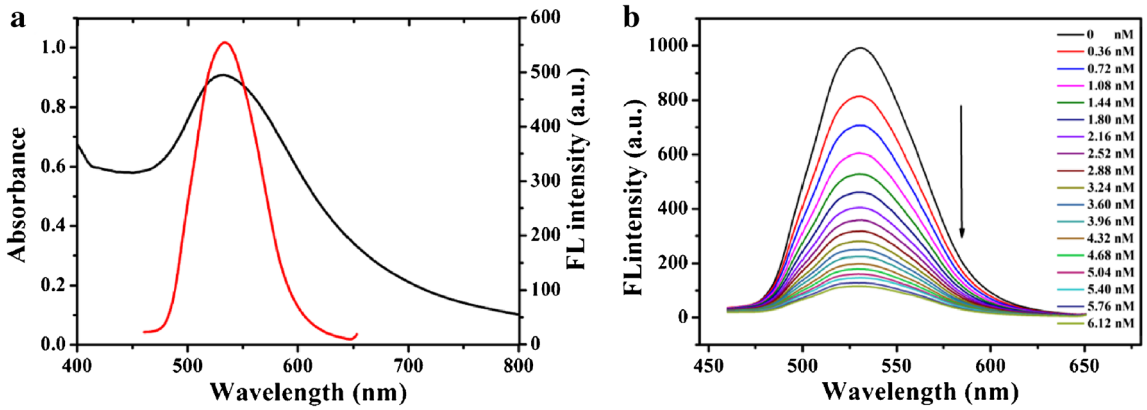

Fig. 3 **a)** The absorption spectrum of Au NPs (blank line) and emission spectrum of N,S-CDs (red line) with the excitation wavelength of 460 nm. **b**) The fluorescence spectra of N,S-CDs (19 μg mL^{-1}) in presence of different concentrations of Au NPs from 0 to 6.12 nM

of Au NPs were investigated, as shown in Fig. 3a. It can be observed that there was a remarkable overlap between the fluorescence emission spectrum of N,S-CDs (red line) and the UV-vis absorption spectrum of Au NPs (black line). Fig. S2 (see the ESM) revealed that the zeta potentials of N,S-CDs and Au NPs were 9.86 and − 6.14 mV at pH 5.0, respectively, which was beneficial for the nearness between N,S-CDs and Au NPs by electrostatic interaction. Therefore, this suggested that N,S-CDs and Au NPs can form an effective FRET donor-acceptor pair in theory.

In order to confirm the occurrence of FRET, the titration experiment of fluorescence spectra of N,S-CDs by Au NPs were investigated, as shown in Fig. 3b. As expected, the fluorescence intensities of N,S-CDs gradually decreased with the increase of Au NPs concentration. The fluorescence of N,S-CDs was quenched nearly 90% while the concentration of Au NPs added to 6.12 nM. It was demonstrated that the energy was successfully transferred from N,S-CDs to Au NPs based on FRET mechanism. Fig. 4 displayed the time-resolved fluorescence spectra of N,S-CDs in the absence and presence of Au NPs, and the fluorescence lifetimes were fitted and listed in Table S1 (see the ESM). The fluorescence lifetime of N,S-CDs followed double-exponential model, that is, N,S-CDs possessed two decay components: a short lifetime component (τ_1) and a long lifetime component (τ_2). The fluorescence lifetime of CDs has been discussed in previous reports [34–36], and it was speculated that the two lifetime components of N,S-CDs may be attributed to the carbon center (or conjugated structures) and surface traps, respectively. The average lifetime of N,S-CDs (τ_D) was calculated to be 9.97. When 6.12 nM Au NPs was added to the N,S-CD solution, the average lifetime of N,S-CDs (τ_{DA}) was calculated to be 3.89 ns. It was revealed that the average lifetimes of the donor (N,S-CDs) significantly decreased with the addition of acceptor (Au NPs), which suggested the dynamic quenching occurred between N,S-CDs and Au NPs. The transfer efficiency of FRET could be calculated according to the following equation:

$$\eta_{FRET} = 1 - \frac{\tau_{DA}}{\tau_D}$$

where τ_D and τ_{DA} are the fluorescence lifetime of donor in the absence or presence of acceptor, respectively. Base on the data of Table S1 (see the ESM), the transfer efficiency was calculated to be 59.1% after adding 6.12 nM Au NPs into 19 μg mL^{-1} N,S-CD solution, which was greatly beneficial to construct the sensing platform.

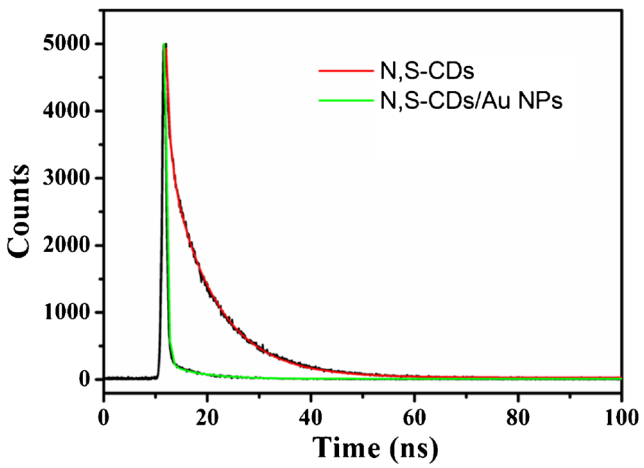

Fig. 4 The fluorescent decay curves of N,S-CDs (19 μg mL^{-1}) in the absence and presence of Au NPs (6.12 nM) at pH 5.0

Fluorescence "turn-on" assay of GSH

The effect of GSH on the FRET system between N,S-CDs and Au NPs was studied. Fig. 5 presents the fluorescence spectra of N,S-CDs (curve a, blank line), N,S-CDs/Au NPs (curve b, red line), and N,S-CDs/Au NPs/GSH (curve c, blue line) under the same experimental conditions. The fluorescence of N,S-CDs (19 μg mL^{-1}) was quenched nearly 90% while the concentration of Au NPs was 6.12 nM. After adding 528.3 μM GSH into the mixture solution of N,S-CDs and Au NPs, it can be observed that the fluorescence intensity of

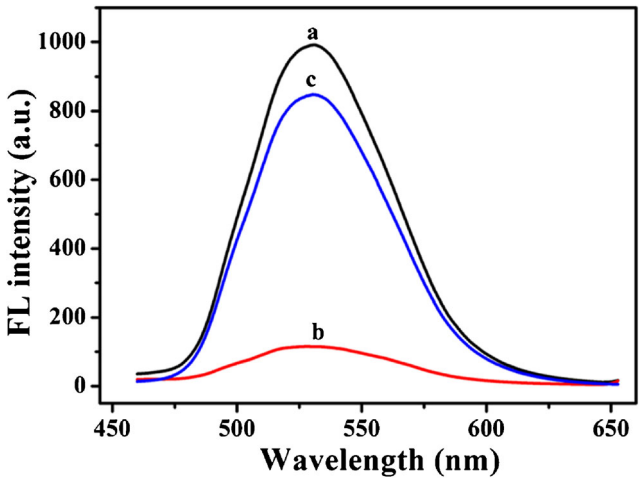

Fig. 5 The fluorescence emission spectra of N,S-CDs (curve a), N,S-CDs/Au NPs (curve b), and N,S-CDs/Au NPs/GSH (curve c)

N,S-CDs was increased significantly, while the emission spectral characteristic was not affected. It was speculated that GSH could bind to Au NPs through strong Au-S bond coordination interaction, resulting in the release of N,S-CDs from the surface of Au NPs. Correspondingly, the FRET process was interrupted and the fluorescence of N,S-CDs was recovered. Furthermore, the zeta potential of GSH at pH 5.0 was 13.2 mV (see ESM Fig. S3), indicating that it was positively charged. It meant that GSH was accessible to the negatively charged Au NPs, facilitating the interaction between GSH and Au NPs and driving Au NPs away from the surface of N, S-CDs by electrostatic repulsion.

The fluorescence spectra of the FRET system in the presence of various concentration of GSH were displayed in Fig. 6a. It can be seen that the fluorescence intensity of N,S-CDs gradually increased with an increasing the concentration of GSH. The changes of fluorescence intensity of N,S-CDs exhibited a linear relationship with the concentration of GSH from 3.8 to 415.1 μM (Fig. 6b). The limit of detection ($3\sigma/s$) for GSH was 0.21 μM, where σ and s represent the standard deviation of 12 blank measurements and the slope of the calibration curve, respectively. The performance of the as-constructed nanosensor platform had a wider linear range than the previous reported GSH detection sensors (see Table 1).

Optimization of the experimental conditions for GSH detection

Considering that some parameters, such as the concentration of AuNPs, pH, and incubation time, had a great influence on the GSH detection, these parameters were thus optimized for preferable analytical performances. Fig. 7a depicted the effect of Au NPs concentration on the fluorescence intensity of N,S-CDs. The emission intensity of N,S-CDs was evidently quenched by Au NPs and nearly kept stable until the concentration of Au NPs reached to 6.12 nM, so the optimal concentration of Au NPs was 6.12 nM. Fig. 7b, c demonstrated that the effect of pH and incubation time on the sensitivity of FRET system for the detection of GSH. The degree of the fluorescence recovery of N,S-CDs/Au NPs/GSH gradually increased when pH varied from 2.0 to 5.0, whereas it decreased sharply when pH > 5.0. So pH 5.0 was selected as the optimal pH for further experiments. Fig. 7c indicated that the fluorescence intensity of the N,S-CDs was quickly recovered from 0 to15 min and gradually become stable from 15 to 50 min. Therefore, in order to guarantee the homogeneity throughout the assay and acquire stable fluorescence signal, 15 min was selected as the optimal incubation time.

Selectivity detection of GSH

It was investigated that the fluorescence response of N,S-CDs/Au NPs nanosensor platform toward GSH and other interferences such as 16 kinds of natural amino acids, Cys, and Hcy. As shown in Fig. S4 (see the ESM) and Fig. 7d, it was evident

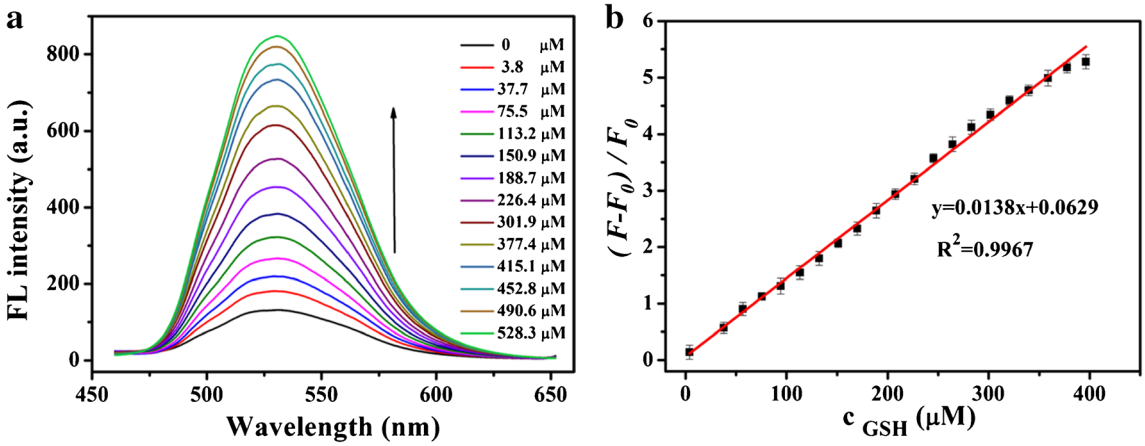

Fig. 6 **a)** The fluorescence spectra of the N,S-CDs/Au NPs in the presence of different concentrations of GSH (0 μM to 528.3 μM). **b)** The linear relationship between the fluorescence changes of N,S-CDs and the concentration of GSH

Table 1 Comparison of different optical nanosensors for GSH determination

Methods	Linear range	LOD	Ref.
EDC/CQD fluorescence	1.0–50.0 μM	0.943 μM	[35]
Binaphthyl aldehyde fluorescence	Not given	1.72 μM	[11]
UCD fluorescence	4.0–9.0 μM	0.066 μM	[12]
Rhodamine colorimetric and fluorescent	5–50 μM	0.17 μM	[7]
C-dots-MnO_2 fluorescence	1–10 μM	300 nM	[16]
CD/AuNP fluorescence	3.8–415.1 μM	0.21 μM	This work

that GSH had the largest fluorescence recovery for FRET system in all tested substances. These results demonstrated that the common co-existing amino acids (without –SH) could not couple with Au NPs, revealing that this FRET-based nanosensor platform was highly selective toward GSH. Only the competitive biothiols (Hcy and Cys) could lead to the fluorescence recovery of the N,S-CDs/Au NPs system to some extent. Nevertheless, the concentration of Hcy and Cys was 7.5 times higher than that of GSH, and the fluorescence recovery of the FRET system by GSH were 9.7 and 10.7 times more than those toward Hcy and Cys, respectively. Besides, the content of Hcy and Cys was much lower than that of GSH in biological systems [37, 38]; these facts showed that the interference can be neglected for this nanosensor platform. Therefore, the nanosensor platform can provide the discriminative recognition of GSH over Cys and Hcy. Moreover, many studies have indicated that GSH has a stronger affinity to Au NPs than Cys and Hcy, because GSH possesses the multi-dentate anchor and the specific steric structure [39].

Determination of GSH in real samples

In order to evaluate the feasibility of the proposed sensing strategy in a complicated environment, GSH in human serum

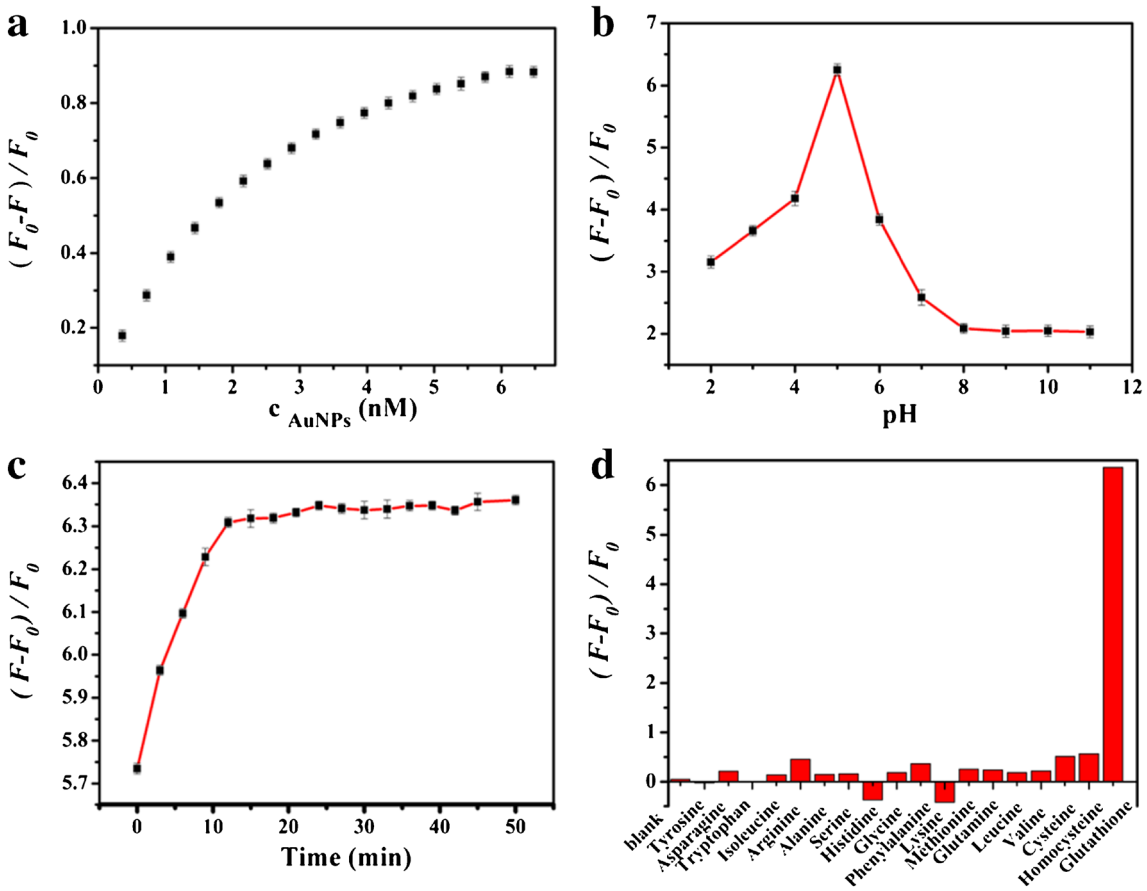

Fig. 7 **a)** The effect of the concentration of Au NPs on the fluorescence intensity of N,S-CDs. The plots of $(F - F_0)/F_0$ against experimental parameters: **b)** pH and **c)** incubation time. F_0 was the fluorescence intensity of N,S-CDs in FRET assembly, F were the fluorescence intensities of N,S-CDs in FRET assembly after adding different concentration of GSH. **d)** The selectivity of the nanosensor platform toward GSH. The concentration of GSH and interferences were 500 μM and 3.77 mM, respectively

Table 2 Determination of GSH in human serum samples

Samples	Found in sample (μM)	Added (μM)	Total found (μM)	Recovery (%)	RSD (%) ($n = 5$)
Human serum 1	2.39	3.77	6.05	97.1	3.10
		7.55	9.12	89.1	4.90
		15.09	16.94	95.8	3.74
Human serum 2	2.21	3.77	5.93	98.7	3.63
		7.55	8.93	89.0	2.77
		15.09	16.78	96.6	3.12

was detected. Because of the concentration of GSH in human serum is up to mM levels, the obtained human serum was diluted to facilitate the concentration of GSH within the linear range of this nanosensor platform. To determinate the recoveries of the nanosensor paltform, different concentrations of GSH (3.77 μM, 7.55 μM, and 15.09 μM) were spiked into the diluted human serum 1 and 2. As shown in Table 2, the recoveries for the detection of GSH were 89.1–97.1% with the relative standard deviations (RSDs) < 4.90% ($n = 5$). These results demonstrated that the proposed nanosensor platform could be used to determinate GSH content in the complex human serum samples with a high degree of simplicity and accuracy and has potential application in actual biomolecules detection.

Conclusions

In summary, a novel "turn-on" sensing platform based on FRET system between N,S-CDs and Au NPs was constructed for the determination of GSH. As the emission spectra of N,S-CDs overlaped excellently with the absorption spectra of Au NPs, and positively charged N,S-CDs and negatively charged Au NPs could be close to each other by electrostatic interaction, an high-efficient FRET process occurred. When GSH was added into the solution of N,S-CDs/Au NPs, the fluorescence intensity of N,S-CDs was significantly recovered. It was speculated that GSH can bind to Au NPs through strong Au-S bond coordination interaction, resulting in the release of N,S-CDs from the surface of Au NPs and the fluorescence recovery of N,S-CDs. The degree of fluorescence recovery was linearly correlated with the concentration of GSH. Therefore, a new method for the quantitative detection of GSH can be established based on this strategy. Selective experiments indicated that the common co-existing amino acids (without –SH) did not interfere with the determination of GSH, and GSH could be discriminatively detected over Cys and Hcy owing to the multi-dentate anchor and the specific steric structure of GSH. The performance was good in the detection of GSH in human serum samples, demonstrating it has potential applications in bioanalysis. Compared with the reported methods, the proposed method possessed superior properties such as higher selective, better sensitivity, lower cost, and easier operation.

Acknowledgments This work was financially supported by the National Natural Science Foundation of China (No. 21705101), Natural Science Foundation of Shanxi Province (No. 201801D121040), and China Postdoctoral Science Foundation (No. 2018M642969).

Compliance with ethical standards

Conflict of interest The authors declare that they have no conflict of interest.

Ethics approval and consent to participate This study conformed to the ethical guidelines of the Declaration of Helsinki and was approved by the Shanxi University Institutional Review Board Office. All human serum samples are supplied by the healthy volunteers with their informed consent.

References

1. Singh VK, Yadav PK, et al. Peroxidase mimetic activity of fluorescent N,S-carbon quantum dots and their application in colorimetric detection of H_2O_2 and glutathione in human blood serum. J Mater Chem B. 2018;6:5256–68.
2. Gao Y, Wu KL, Li HY, Chen W, Fu M, Yue K, et al. Glutathione detection based on peroxidase-like activity of Co_3O_4-montmorillonite nanocomposites. Sensors Actuators B Chem. 2018;273:1635–9.
3. Wu R, Ge HG, Liu CF, Zhang SH, Hao L, Zhang Q, et al. A novel thermometer-type hydrogel senor for glutathione detection. Talanta. 2019;196:191–6.
4. Peng HP, Jian ML, Huang ZN, Wang WJ, Deng HH, Wu WH, et al. Facile electrochemiluminescence sensing platform based on high-quantum yield gold nanocluster probe for ultrasensitive glutathione detection. Biosens Bioelectron. 2018;105:71–6.
5. Chen W, Zhao Y, Seefeldt T, Guan X. Determination of thiols and disulfides via HPLC quantification of 5-thio-2-nitrobenzoic acid. J Pharm Biomed. 2008;48:1375–80.
6. Saha A, Jana NR. Detection of cellular glutathione and oxidized glutathione using magnetic-plasmonic nanocomposite based turn-off surface enhanced Raman scattering. Anal Chem. 2013;85:9221–8.
7. Chen LY, Jong SP, Wu D, Cheol HK, Yoon JY. A colorimetric and fluorescent probe for rapid detection of glutathione and its application to tissue specific bioimaging in living cells and zebrafish. Sensors Actuators B Chem. 2018;262:306–12.

8. Burford N, Eelman MD, Mahony DE, Morash M. Definitive identification of cysteine and glutathione complexes of bismuth by mass spectrometry: assessing the biochemical fate of bismuth pharmaceutical agents. Chem Commun. 2003;14:146–7.
9. Hodáková J, Preisler J, Foret F, Kubán P. Sensitive determination of glutathione in biological samples by capillary electrophoresis with green (515 nm) laser-induced fluorescence detection. J Chromatogr A. 2015;1391:102–8.
10. Wawegama NK, Browning GF, Kanci A, Marenda MS, Markham PF. Development of a recombinant protein-based enzyme-linked immunosorbent assay for diagnosis of Mycoplasma bovis infection in cattle. Clin Vaccine Immunol. 2014;21:196–202.
11. Chen W, Wu XD, Pu L. Highly selective fluorescent recognition of glutathione by using a water soluble binaphthyl aldehyde. Tetrahedron Lett. 2017;58:1781–3.
12. Qin J, Zhang LM, Yang R. Powder carbonization to synthesize novel carbon dots derived from uricacid for the detection of Ag(I) and glutathione. Spectrochim Acta A Mol Biomol Spectrosc. 2019;207:54–60.
13. Niu LY, Guan YS, Chen YZ, Tung CH, Yang QZ. BODIPY-based ratiometric fluorescent sensor for highly selective detection of glutathione over cysteine and homocysteine. J Am Chem Soc. 2012;134:18928–31.
14. Shao N, Jin J, Wang H, Zheng J, Yang R, Chan W, et al. Design of bis-spiropyran ligands as dipolar molecule receptors and application to in vivo glutathione fluorescent probes. J Am Chem Soc. 2010;132:725–36.
15. Yang CL, Deng WP, Liu HY, Ge SG, Yan M. Turn-on fluorescence sensor for glutathione in aqueous solutions using carbon dots–MnO_2 nanocomposites. Sensors Actuators B Chem. 2015;216:286–92.
16. Cai QY, Li J, Ge J, Zhang L, Hu YL, Li ZH, et al. A rapid fluorescence "switch-on" assay for glutathione detection by using carbon dots-MnO_2 nanocomposites. Biosens Bioelectron. 2015;72:31–6.
17. Xiang HJ, Tham HP, Nguyen MD, Phua SZF, Lim WQ, Liu JG, et al. An aza-BODIPY based near-infrared fluorescent probe for sensitive discirmination of cysteine/homocysteine and glutathione in living cells. Chem Commun. 2017;53:5220–3.
18. Deng JH, Lu QJ, Hou YX, Liu ML, Li HT, Zhang YY, et al. Nanosensor composed of nitrogen-doped carbon dots and gold nanoparticles for highly selective detection of cysteine with multiple signals. Anal Chem. 2015;87:2195–203.
19. Zhang Q, Gong Y, Guo XJ, Zhang P, Ding CF. Multifunctional gold nanoparticle-based fluorescence resonance energy-transfer probe for target drug delivery and cell fluorescence imaging. ACS Appl Mater Interfaces. 2018;10:34840–8.
20. Han X, Han M, Ma L, Qu F, Kong RM, Qu FL. Self-assembled gold nanoclusters for fluorescence turn-on and colorimetric dual-readout detection of alkaline phosphatase activity via DCIP-mediated fluorescence resonance energy transfer. Talanta. 2019;194:55–62.
21. Wang J, Song FJ, Ai YL, Hu SW, Huang ZZ, Zhong WY. A simple FRET system using two-color CdTe quantum dots assisted by cetyltrimethylammonium bromide and itsapplication to Hg(II) detection. Lumin. 2019;34:205–11.
22. Chen GW, Song FL, Xiong XQ, Peng XJ. Fluorescent nanosensors based on fluorescence resonance energy transfer (FRET). Ind Eng Chem Res. 2013;52:11228–45.
23. Jing N, Tian M, Wang YT, Zhang Y. Nitrogen-doped carbon dots synthesized from acrylic acid andethylenediamine for simple and selective determination of cobalt ions in aqueous media. J Lumin. 2019;206:169–75.
24. Gong XJ, Li ZB, Hu Q, Zhou RX, Shuang SM, Dong C. N,S,P Co-doped carbon nanodot fabricated from waste microorganism and its application for label-free recognition of manganese(VII) and L-ascorbic acid and and logic gate operation. ACS Appl Mater Interfaces. 2017;9:38761–72.
25. Ding H, Zhou XX, Qin BT, Zhou ZY, Zhao YP. Highly fluorescent near-infrared emitting carbon dots derived from lemonjuice and its bioimaging application. J Lumin. 2019;211:298–304.
26. Ahmed SR, Kim J, Suzuki T, Lee J, Park EY. Enhanced caalytic activity of gold nanoparticle-carbon nanotube hybrids for influenza virus detection. Biosens Bioelectron. 2016;85:503–8.
27. Yang YX, Huo DQ, Wu HX, Wang XF. N, P-doped carbon quantum dots as a fluorescent sensing platform for carbendazim detection based on fluorescence resonance energy transfer. Sensors Actuators B Chem. 2018;274:296–303.
28. Wu XL, Song Y, Yan X, Zhu CZ, Ma YQ, Du D, et al. Carbon quantum dots as fluorescence resonance energy transfer sensors for organophosphate pesticides determination. Biosens Bioelectron. 2017;94:292–7.
29. Niu WJ, Shan D, Zhu RH, Deng SY, Ceng S, Zhang XJ. Dumbbell-shaped carbon quantum dots/AuNCs nanohybrid as an efficient ratiometric fluorescent probe for sensing cadmium (II) ionsand L-ascorbic acid. Carbon. 2016;96:1034–42.
30. Meng FY, Chai H, Ma XY, Tang YG, Miao P. FRET investigation toward DNA tetrahedron-based ratiometric analysis of intracellular telomeraseactivity. J Mater Chem B. 2019;7:1926–32.
31. Shi J, Chan C, Pang Y, Ye W, Tian F, Lyu J, et al. A fluorescence resonance energy transfer (FRET) biosensor based on graphene quantum dots (GQDs) and gold nanoparticles (AuNPs) for the detection of mecA gene sequence of Staphylococcusaureus. Biosens Bioelectron. 2015;67:595–600.
32. Zhao WA, Brook MA, Li YF. Design of gold nanoparticle-based colorimetric biosensing assays. Chembiochem. 2008;9:2363–71.
33. Gong XJ, Wang HP, Liu Y, Hu Q, Gao YF, Yang ZH, et al. A difunctional and label-free carbon-based chem-nanosensor for real-time monitoring of pH fluctuation and quantitative determining of curcumin. Anal Chim Acta. 2019;1057:132–44.
34. Fan RJ, Sun Q, Zhang L, Zhang Y, Lu AH. Photoluminescent carbon dodirectly derived from polyethylene glycol and their application for cellular imaging. Carbon. 2014;71:87–93.
35. Kalytchuk S, Polakova K, Wang Y, Froning JP, Cepe K, Rogach AL, et al. Carbon dot nanothermometry: intracellular photoluminescence lifetime thermal sensing. ACS Nano. 2017;11:1432–42.
36. Jovin TM, Wieb van der Meer B, Hildebrandt N, Sapsford KE, Pons T, Campbell RE, et al. Outlook on FRET: the future of resonance energy transfer. FRET—Förster resonance energy transfer. Wiley-VCH; 2013. p. 757–65.
37. Yu FB, Li P, Wang BS, Han KL. Reversible near-infrared fluorescent probe introducing tellurium to mimetic glutathione peroxidase for monitoring the redoxcycles between peroxynitrite and glutathione in vivo. J Am Chem Soc. 2013;135:7674–80.
38. Pan JH, Zheng ZY, Yang JY, Wu YY, Lu FS, Chen YW, et al. A novel and sensitive fluorescence sensor for glutathione detection by controlling the surface passivation degree of carbon quantum dots. Talanta. 2017;166:1–7.
39. Shi Y, Pen Y, Zhang H, Zhang Z, Li MJ, Yi C, et al. A dual-mode nanosensor based on carbon quantum dots and gold nanoparticles for discriminative detection of glutathionein human plasma. Biosens Bioelectron. 2014;56:39–45.